frontiers | Frontiers in Mechanical Engineering

ORIGINAL RESEARCH
published: 29 April 2022
doi: 10.3389/fmech.2022.888350

Uniformity Prediction of Bending Stiffness of Composite Space Mirrors With Ply Angle Misalignments by Deflection Angle

Qingnian Liu[1,2,3], *Yingfeng Shao*[1], *Long Li*[1]*, *Yong Cai*[4] *and Fan Song*[1,3]*

[1]State Key Laboratory of Nonlinear Mechanics (LNM) and Beijing Key Laboratory of Engineered Construction and Mechanobiology, Institute of Mechanics, Chinese Academy of Sciences, Beijing, China, [2]The System Design Institute of Mechanical—Electrical Engineering, Beijing, China, [3]School of Engineering Science, University of Chinese Academy of Sciences, Beijing, China, [4]Aerospace Research Institute of Materials and Processing Technology, Beijing, China

Based on the classical lamination theory, the principal moment direction of the laminate is derived. It is 45° apart from the generalized ply angle, which is the orientation of the ply where the ply angle misalignment occurs nominally. After adding a fixed one-ply angle or random multiple ply angle misalignments to six quasi-isotropic and symmetric stacking sequences, out-of-plane deformations of mirrors were simulated and compared. The result shows an angle difference between the principal moment and curvature directions. It is referred to as the deflection angle, approximately appearing as a trigonometric curve, which varies with laminates and is dependent on the generalized ply angle within each laminate. The deflection angle directly reflects the consistency of bending stiffness or laminate bending anisotropy; the smaller the deflection angle, the better will be the uniformity of bending stiffness. Consequently, it is an efficient approach to obtain a laminate with more uniformity of bending stiffness by comparing the deflection angle. These results enrich the research of out-of-plane deformation and could objectively promote the study of quasi-isotropic laminates for bending stiffness.

Keywords: carbon fiber–reinforced polymer, bending stiffness, ply angle misalignment, principal direction, generalized ply angle, deflection angle

OPEN ACCESS

Edited by:
Zhaohe Dai,
University of Oxford, United Kingdom

Reviewed by:
Yu-Sheng Lo,
Cadence Design Systems, United States
Xiaojie Ma,
Peking University, China

***Correspondence:**
Long Li
lilong@lnm.imech.ac.cn
Fan Song
songf@lnm.imech.ac.cn

Specialty section:
This article was submitted to Solid and Structural Mechanics, a section of the journal Frontiers in Mechanical Engineering

Received: *02 March 2022*
Accepted: *28 March 2022*
Published: *29 April 2022*

Citation:
Liu Q, Shao Y, Li L, Cai Y and Song F (2022) Uniformity Prediction of Bending Stiffness of Composite Space Mirrors With Ply Angle Misalignments by Deflection Angle. Front. Mech. Eng 8:888350. doi: 10.3389/fmech.2022.888350

1 INTRODUCTION

Carbon fiber–reinforced polymer (CFRP) is primarily composed of reinforcements and matrices with different chemical and physical properties (Yi et al., 2018; Ma et al., 2020). CFRP has superior performance, such as low density, high specific strength, high specific modulus, and low thermal expansion, which leads to an increasing variety of structural applications, ranging from aerospace and automobile to civil infrastructure and sports (Xie et al., 2016; Chen et al., 2021; Song and Jin, 2021; Różyło and Dębski, 2022).

CFRP is adopted as one of the most competitive materials for the space mirror, which requires hygrothermal stability and high specific stiffness to retain high precision for a long term since it should be exposed to the temperature cycle endlessly during its employment (Wei et al., 2017; Yoon et al., 2014). Compared with conventional materials, CFRP could potentially manufacture the larger mirror to match the growing demand for high resolution, owing to its lightweight (Kim and Hale, 2010; Steeves and Pellegrino, 2017; Tanaka et al., 2016). One of the greatest advantages of CFRP is its tailoring which could

lead to quasi-isotropy by appropriate stacking sequences with the unidirectional CFRP (Bruyneel et al., 2012; Thompson et al., 2014; Wu and Avery, 1992). Then, CFRP usually was used to manufacture the macroscopic isotropic mirror. Unexpectedly there was always the unpredicted out-of-plane deformation after curing where existed the temperature change even if the laminate was symmetric in both geometry and material properties about the middle surface (Chen et al., 2000; Verchery, 2011; Yang et al., 2018). Its anomalous behavior could not happen to any isotropic materials, and one of the possible reasons is the ply angle misalignments during stacking layer by layer (Arao et al., 2011; Cheng et al., 2021; Wilhelmsson et al., 2020). In particular, there are ply angle misalignments between the actual and designed laminate, which is inevitable whether plies are laid by manual prepreg lay-up or automated tape lay-up (Liu et al., 2019; Yang et al., 2019).

Many researchers investigated the relationship between out-of-plane deformation and the ply angle misalignment and improved mirrors' accuracy. Using simulation, Thompson et al. (2014) and Yang et al. (2019) formulated that the surface peak-to-valley (PV) was proportional to the magnitude of the ply angle misalignment and the area of mirrors. Liu et al. (2019) suggested that PV was associated with the consistency of the bending stiffness matrix; in other words, the better the uniformity of bending stiffness, the smaller will be the out-of-plane deformation resulting from the identical multiple ply angle misalignments. It could be inferred that decreasing the ply thickness, increasing the ply number, and raising the uniformity of the bending stiffness matrix could improve the accuracy of the space mirror when the angle misalignment occurs. However, these qualitative conclusions nearly have little effect on optimizing the constant bending stiffness of laminates, which is the vital factor affecting the precision of the space mirror. Then, the direction of the out-of-plane deformation is likely the investigation field to improve the uniformity of the bending stiffness. Tanaka et al. (2016) presented that the direction of the maximum and minimum displacements just rotated ± 45° from the orientation of one ply, where the angle misalignment occurred. Unluckily, the derivation was not strict because the saddle-shaped mirror was primarily caused by moments, not forces, so that conclusion did not match the practical condition.

In addition, many researchers directly pay attention to investigate the fully isotropic laminates since they could decrease the effect of the ply angle misalignment to some extent (Fukunaga, 1990; Fukunaga and Sekine, 1992; Wu and Avery, 1992; Vannucci and Verchery, 2002). For example, Yang et al. (2018)and Yang et al. (2019) presented the method of the regularization stiffness coefficient and coefficients of bending/twisting to optimize stacking sequences, respectively. However, their objective functions are subjective, especially on the weight factors, so their optimization laminates were quite different. The advantages and disadvantages of these methods were too hard to be directly verified.

Accordingly, to compensate the lack of objective research on fully isotropic laminates and improve the mirror's accuracy, it is urgent to investigate more accurate directions or positions of maximum and minimum displacements resulting from one-ply or multiple ply angle misalignments. Consequently, in this study, based on the angle misalignment, we studied two principal directions, the principal moment direction and the principal curvature direction, and investigated the relationship between the difference of two principal directions and the uniformity of the bending stiffness. In addition, we found the deflection angle, the difference of two principal directions, is an inherent property of the laminate and could be regarded as an objective function to optimize the laminate of constant bending stiffness.

2 THEORETICAL ANALYSIS

2.1 Resultant Thermal Moment

A symmetric laminate with n plies and the constant ply thickness δ is considered. The uniform temperature change, ΔT, is acted on it, and then, the resultant thermal moment (Cheng et al., 2021) is expressed as follows:

$$\{M^T\} = \frac{1}{2}\left[\bar{Q}\right]_k \{\bar{\alpha}\}_k \Delta T\left(z_k^2 - z_{k-1}^2\right) = \Delta T \delta [Q]\{\alpha\}\sum_{k=1}^{n} d_k [T]_k^{-1}, \quad (1)$$

where $[T]$ is the transformation matrix, $[Q]$ and $[\bar{Q}]$ are the on-axis and off-axis stiffness matrices, and $\{\alpha\}$ and $\{\bar{\alpha}\}$ are the on-axis and off-axis coefficients of thermal expansion, respectively. The k^{th} ply extends from z_{k-1} to z_k, and d_k is the transverse coordinates of the middle surface of the k^{th} ply (as shown schematically in **Figure 1**). With respect to the symmetric laminate, $[T]$ and d_k follow as

$$d_k = -d_{n+1-k}, \left(T_{ij}^{-1}\right)_k = \left(T_{ij}^{-1}\right)_{n+1-k}. \quad (2)$$

Combined with the aforementioned equation, **Eq. 1** is simplified to $\{M^T\} = 0$. In particular, the resultant thermal moment is eliminated for the symmetric laminate subjected to the uniform temperature change. By virtue of the partial derivative with **Eq. 1**, the increment of the resultant thermal moment resulting from the k^{th} ply unit angle misalignment is achieved as follows:

$$\begin{aligned}\{\Delta M^T\}_k &= \frac{\partial\{M^T\}}{\partial\theta_k} = \Delta T \delta d_k \frac{d[T]^{-1}}{d\theta}|_k [Q]\{\alpha\} \\ &= \delta \Delta T p\{-m_{2k} m_{2k} m_{1k}\}^T, \end{aligned} \quad (3)$$

where the superscript T on the outside of the brackets indicates the transpose, and

$$m_{1k} = d_k \cos 2\theta_k, m_{2k} = d_k \sin 2\theta_k, \quad (4)$$

where θ_k denotes the orientation of ply k, and m_{1k} and m_{2k} are the twisting moment component and the bending moment component of the resultant thermal moment resulting from the unit angle misalignment of the k^{th} ply, respectively. p is a comprehensive material parameter associated with coefficients of stiffness, Q_{ij}, and coefficients of thermal expansion, α_i, and its expression is as follows:

$$p = Q_{11}\alpha_1 + Q_{12}\alpha_2 - Q_{12}\alpha_1 - Q_{22}\alpha_2. \quad (5)$$

According to **Eq. 3** or **Eq. 4**, the magnitude of the resultant thermal moment is proportional to the transverse coordinate of the center surface of the ply where the ply angle misalignment

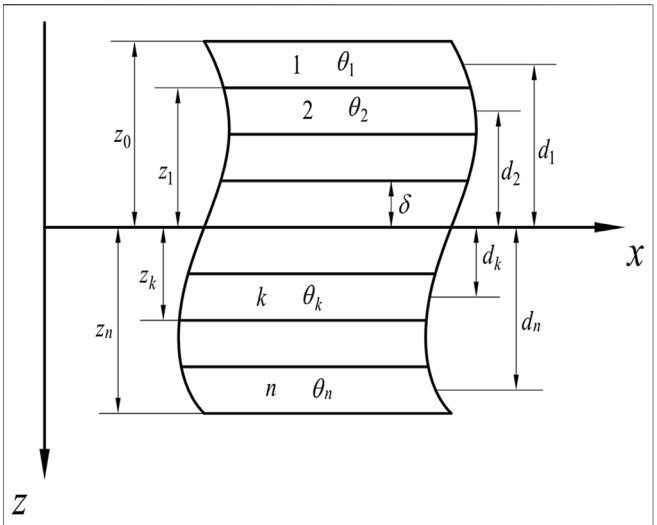

FIGURE 1 | Coordinate system and the ply number for a laminate. θ_k denotes the orientation of ply k, and each ply is of constant thickness, δ. z_{k-1}, d_k, and z_k are the transverse coordinates of the top, middle, and bottom surface of the k^{th} ply, respectively.

occurs and the magnitude of the ply angle misalignment (Liu et al., 2019). For multi-ply angle misalignments, the total increment of the resultant thermal moment is the sum of aforementioned two formulas multiplied associated ply angle misalignments:

$$\{\Delta M^T\} = \sum_{k=1}^{n}\{\Delta M^T\}_k \Delta\theta_k = \delta\Delta T p_2 \sum_{k=1}^{n}\Delta\theta_k\{-m_{2k}\, m_{2k}\, m_{1k}\}^T$$
$$= \delta\Delta T p_2\{-m_2\, m_2\, m_1\}^T, \quad (6)$$

where

$$m_1 = \sum_{k=1}^{n} m_{1k}\Delta\theta_k = \sum_{k=1}^{n} d_k \cos 2\theta_k \Delta\theta_k,$$
$$m_2 = \sum_{k=1}^{n} m_{2k}\Delta\theta_k = \sum_{k=1}^{n} d_k \sin 2\theta_k \Delta\theta_k. \quad (7)$$

Similarly, m_1 and m_2 are the twisting moment and the bending moment components of the thermal moment resulting from multiple ply angle misalignments, respectively. In consideration of zero thermal moment without the ply angle misalignment, the increment of the resultant thermal moment is replaced by thermal moments in the following text.

According to **Eq. 6**, apparently, the bending moment components around the x-axis and y-axis are identical but have opposite signs. All moment components in an inclined section form a tensor, including stresses and curvatures (Gere and Goodno, 2012; Hyer, 1981; Ugural, 2009). Simultaneously, one of bending moments, such as M_x or M_y, and the twisting moment are just two components of a vector from **Eq. 4**. **Eq. 7** could also be regarded as the vector addition, from which we could conclude thermal moments resulting from multiple ply angle misalignments, also followed by the parallelogram law (Liu et al., 2019).

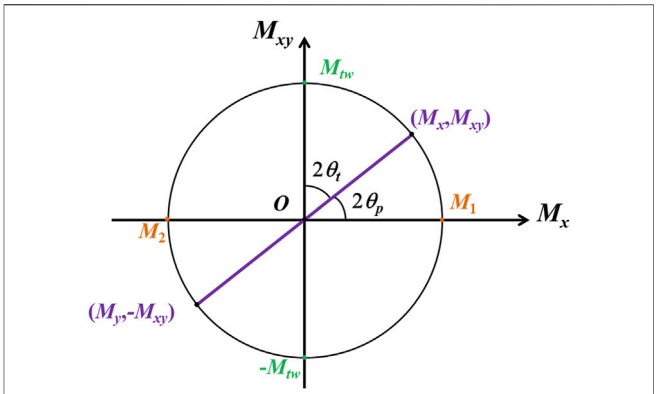

FIGURE 2 | Construction of Mohr's circle for the thermal moment resultant from ply angle misalignments. In the initial ply reference orientation, there are the bending moments M_x and M_y and the twisting moment concurrently; in an inclined surface with rotation angle θ_t (or θ_p) in fact and $2\theta_t$ (or $2\theta_p$) in figure, there is only the maximum twisting moment M_{tw} (or the principal moment M_1 and M_2).

2.2 Principal Directions of the Resultant Thermal Moment

Similar to the stress tensor, the resultant thermal moment also follows Mohr's circle. According to **Eq. 7**, two bending moments are equated to each other and have opposite signs, and then, the center of the circle locates at the origin of the coordinate, as shown in **Figure 2**, a simplified version of Mohr's circle. If the ply reference orientation rotates counterclockwise through an angle θ, then according to **Eq. 7**, the new resultant thermal moment would be as follows:

$$m'_1 = \sum_{k=1}^{n} d_k \cos 2(\theta_k - \theta)\Delta\theta_k, m'_2 = \sum_{k=1}^{n} d_k \sin 2(\theta_k - \theta)\Delta\theta_k. \quad (8)$$

Let's set $m'_2 = 0$ in **Eq. 8**, then the rotation angle θ_t in **Figure 2** could be given as follows:

$$\tan 2\theta_t = m_2/m_1. \quad (9)$$

Similarly, let's set $m'_1 = 0$ in **Eq. 8**, and the rotation angle θ_p (as shown in **Figure 2**) is as follows:

$$\tan 2\theta_p = -m_1/m_2. \quad (10)$$

The angle θ_p is the principal moment direction. It is well known that two values at the circumference match with **Eq. 9**, **10**, respectively. As customary θ_{p1} and θ_{p2} indicate directions of maximum and minimum principal moments when the corresponding m_2 is greater and less than zero, θ_{t1} and θ_{t2} represented orientations of maximum positive and negative twisting moments. Directions after rotating twice of the preceding two rotation angles are parallel to each other, or the difference between two rotation angles is 45°.

In addition, m_1 and m_2 are independent of the temperature change. The rotation angles, θ_t and θ_p, are not correlated with the temperature change and are just dependent on stacking sequences and ply angle misalignments. In other words, for symmetric and quasi-isotropic laminates, the principal moment direction is a

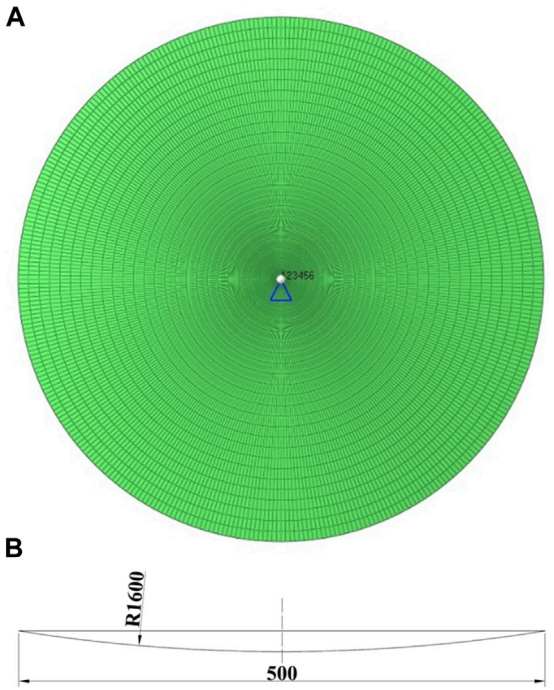

FIGURE 3 | Model of the space mirror. **(A)** Finite element with the fixed center point and **(B)** Front view.

particular property of the laminate with regard to ply misalignments. It remains unchanged during curing inside the autoclave or under temperature cycles in the space environment.

If only one-ply angle misalignment occurs, **Eq. 9** is simplified to the following:

$$\tan 2\theta_t = \tan 2\theta_k. \tag{11}$$

According to the preceding statement, the abovementioned formula indicates that one direction of the maximum twisting moments is parallel to the k^{th} ply orientation and the other is perpendicular to that, and the principal moment directions are always orientated at ± 45° from that, namely, as shown below:

$$\theta_t = \theta_k \, or \, \theta_k + \pi/2, \theta_p = \theta_k \pm \pi/4. \tag{12}$$

Furthermore, for multiple ply angle misalignments θ_t can be gained by **Eq. 9**, which also indicates the direction of maximum or minimum twisting moment. To better distinguish them from θ_t, we defined the generalized ply angle, denoted as θ_G, where the ply angle misalignment occurs nominally, the twisting moment locates at the peak or valley, and is 45° apart from principal moment directions.

3 SIMULATION ANALYSIS

3.1 Material and Model

The model is shown in **Figure 3**, a concave mirror, 2.4 mm thick, with a diameter of 500 mm intercepted from a spherical surface of radius 1,600 mm. There are 9,000 elements, and the angle of each element in the circular direction is approximately 1°. It is made of the carbon fiber composite M40/602, and its properties are detailed in **Table 1**. In total, six freedoms of its center are fixed, and the mirror was only subjected to the thermal load, $\Delta T = -100$°C, uniformly cooling from the curing temperature (125°C) to the room temperature (25°C). In addition, the ply reference direction was along the x-axis, y-axis was 90° direction, and normal direction was along the z-axis. This definition ensured that the angles in the coordinate were consistent with the ply angles.

3.2 Stacking Sequences

A total of six quasi-isotropic and symmetric stacking sequences (shown in **Table 2**) (Liu et al., 2019) were used to simulate out-of-plane deformations with ply angle misalignments. The stacking sequence with ply angle misalignments is regarded as part of the material property in Abaqus. For the symmetric laminate $[B] = 0$, the in-plane and out-of-plane deformations were independent of each other. Concerning the quasi-isotropic laminate, the equivalent coefficients of thermal expansion were identical at the circumference. Therefore, the space mirror should be expanded slightly and uniformly in-plane during its curing process and the temperature cycle in the space environment, and it was usually neglected in consideration of the out-of-plane deformation.

TABLE 1 | Material properties of the unidirectional carbon fiber composite M40J/602.

Material	E_1/GPa	E_2/GPa	G_{12}/GPa	G_{23}/GPa	v	α_{11}/ 10^{-6}°C^{-1}	α_{22}/ 10^{-6}°C^{-1}
M40J/E602	210	7.5	5.69	6.0	0.30	−0.68	32.37

TABLE 2 | Typical stacking sequences.

No.	Lamina thickness/mm	Stacking sequence
1	0.10	$[(60/0/-60)_S]_4$
2	0.10	$[(0/30/60/90/-60/-30)_S]_2$
3	0.10	$[0/15/30/45/60/75/90/-75/-60/-45/-30/-15]_S$
4	0.075	$[(45/0/-45/90)_S]_4$
5	0.075	$[(22.5/90/-45/-22.5/67.5/-67.5/0/45)_S]_2$
6	0.075	$[0/90/45/-45/11.25/-78.75/56.25/-75/22.5/-67.5/67.5/-22.5/33.75/-56.25/78.75/-11.25]_S$

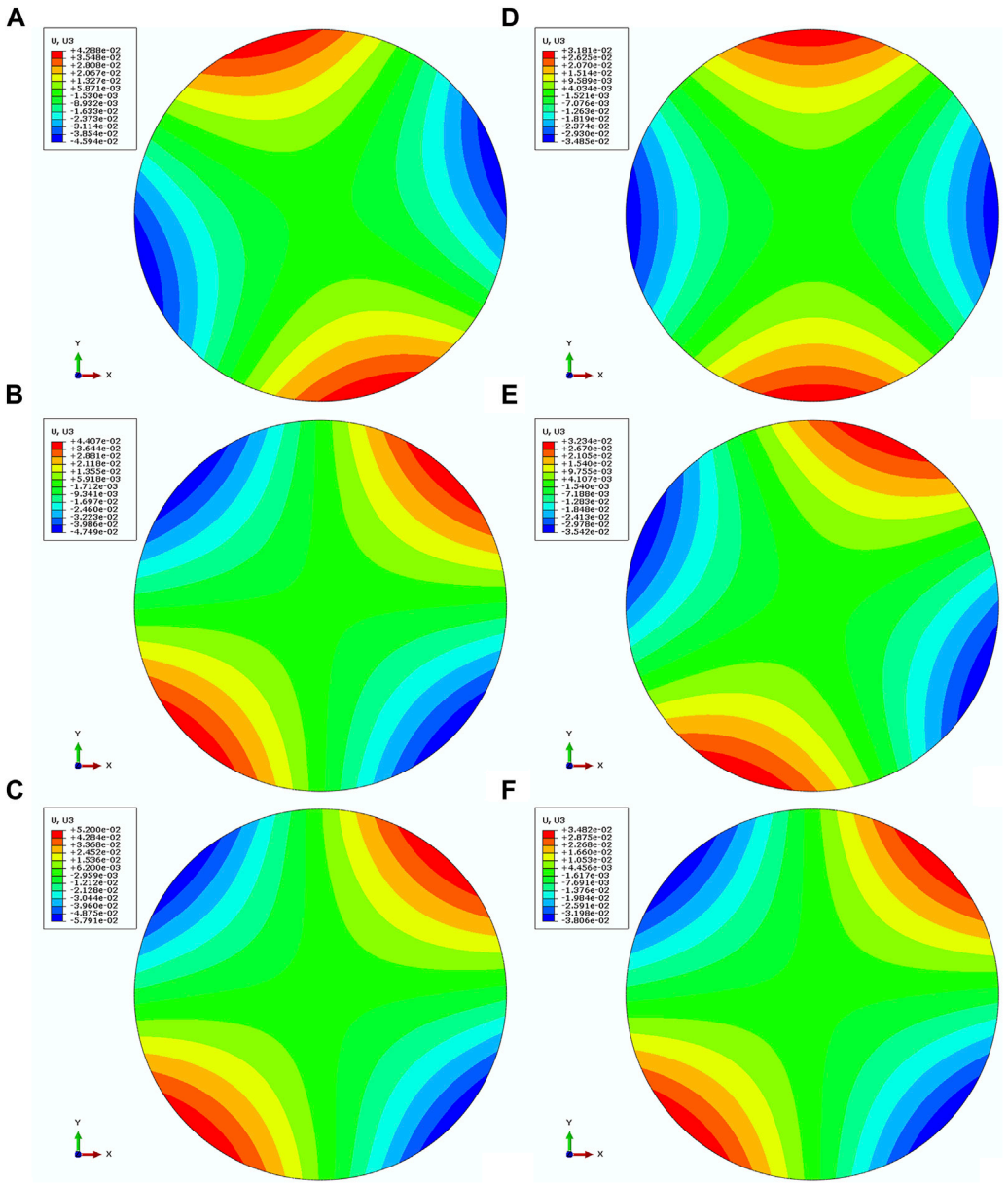

FIGURE 4 | Out-of-plane deformation for six stacking sequences with unit ply angle misalignment in the first layer. **(A)** Stacking No. 1; **(B)** Stacking No. 2; **(C)** Stacking No. 3; **(D)** Stacking No. 4; **(E)** Stacking No. 5; **(F)** Stacking No. 6.

The first three stacking sequences all had 24 layers with the ply thickness of 0.1 mm but different ply angles, namely, 3, 6, and 12 angles in turn, and the last three stacking sequences, which had 32 layers, were 0.075 mm in thickness, and the number of the ply orientations were 4, 8, and 16, respectively.

4 RESULTS AND DISCUSSION

4.1 Fixed Ply Angle Misalignment

The fixed ply angle misalignment, unit angle 1°, is allowed to occur on the first layer, and then, the mirrors' response to the thermal load is calculated. **Figure 4** shows displacement contours in the z-axis direction. Compared with **Table 2**, each displacement contour takes on a saddle shape, and there are two peaks and two valleys separated from each other. According to the differential geometry principle, two peaks corresponded to the maximum curvature, κ_1, and two valleys corresponded to the minimum curvature, κ_2 (as shown in **Figure 5**). Meanwhile, there exists another typical curvature, the maximum twisting curvature, κ_{tw}, was located on the angular bisector of the maximum and minimum curvature.

Extract displacement reports and the associated angles could be achieved through coordinates of nodes, and the effect of in-

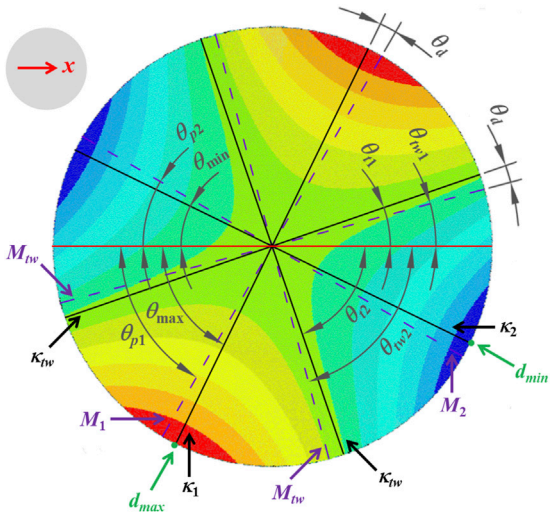

FIGURE 5 | Diagram of principal moments and curvatures, the maximum twisting moment and curvature, and the deflection angle. d_{max} and d_{min} denote the maximum and minimum displacements, respectively. The black solid lines are the principal curvatures, κ_1 and κ_2, the maximum twisting curvature, κ_{tw}, and the corresponding directions are the maximum and minimum principal curvature directions, θ_{max} and θ_{min}, and the direction of the maximum twisting curvatures, θ_{tw1} and θ_{tw2}; the purple dotted lines are the principal moments, M_1 and M_2, the maximum twisting moment, M_{tw}, and the corresponding directions are the maximum and minimum principal moment directions, θ_{p1} and θ_{p2}, and the directions of the maximum twisting curvature, θ_{t1} and θ_{t2}.

plane displacements was ignored. Data are listed in **Table 3**. Directions of κ_1, κ_2, and κ_{tw} are indicated as θ_{max}, θ_{min}, and θ_{tw}, respectively. In addition, the maximum and minimum displacements are expressed as d_{max} and d_{min} (as shown in **Figure 5**).

In **Table 3**, the 2nd column, θ_G, has been achieved by **Eq. 9**, and the 7th column, θ_{tw}, is the average of the 4th and 6th columns. The last column shows differences between the direction of the maximum twisting curvature and the generalized ply angle, which are hardly equal to 0° but only closer to 0°. The angle of each grid is approximately 1°, and the calculation accuracy is about 0.5°. All six results still exceed the angle range of 0° even considering the accuracy of the grid. Therefore, the direction of the maximum twisting curvature is different from that of the generalized ply angles, and this difference is named the deflection angle θ_d.

TABLE 4 | Deflection angle ranges of six stacking sequences with unit ply angle misalignment in each layer at one time.

Stacking No.	Min deflection angle/°	Max deflection angle/°
1	0.00	1.00
2	−1.00	2.00
3	−5.00	7.00
4	1.00	1.00
5	0.00	2.00
6	−2.75	4.25

Furthermore, the fixed ply angle misalignment, unit angle 1°, is allowed to occur on any ply and only one ply at a time, instead of just the first ply, and deformations and analysis deflection angles are calculated. The min and max deflection angles for six stacking sequences are shown in **Table 4**. It indicates that the deflection angle range varies with each stacking sequence. All deflection angles for Stacking No. 2 are detailed in **Table 5**. When the generalized ply angles are 0°, 30°, and −30°, the corresponding deflection angles are just equal to 1°, −1°, and 2°, respectively. For the other stacking sequences, we can also obtain similar results. Meanwhile, the deflection angles of Stacking No. 4 are always 1° (as shown in **Table 4**). Therefore, the deflection angle also changes with the generalized ply angle within each laminate. In other words, deflection angles remain constant for the same generalized ply angle.

If the influence of ply angle misalignments on the stiffness matrix is ignored, for the symmetric laminate, the curvature and the moment followed by $\{\kappa\} = [D]^{-1}\{M^T\}$. In consideration of the same k^{th} ply with the fixed ply angle misalignment, according to **Eq. 7**, the magnitudes of the resultant thermal moment from Stacking No. 1 to Stacking No. 3 are identical to each other, as well as that from Stacking No. 4 to No. 6, and they locate at each generalized ply angle. Then, differences between out-of-plane deformations, including principal curvature directions and deflection angles, could be attributed to the bending stiffness matrix. So the deflection angle is closely related to the bending stiffness matrix.

Furthermore, for the uniform bending stiffness or the isotropic material, the principal curvature directions are always consistent with the principal moment directions. Consecutively, when the deflection angle exists, the bending stiffness at the circumference changes gradually. In other words, the deflection angle reflects the

TABLE 3 | Results of the generalized ply angles and angles of minimum and maximum displacements with unit ply angle misalignment in the first layer.

Stacking No.	θ_G/°	Minimum displacement		Maximum displacement		θ_{tw}/°	$\theta_d = \theta_{tw} - \theta_G$/°
		d_{min}/mm	θ_{min}/°	d_{max} /mm	θ_{max}/°		
1	60.0	−0.0459	16.0	0.0429	−74.0	61.0	1.0
2	0.0	−0.0475	−44.0	0.0441	46.0	1.0	1.0
3	0.0	−0.0579	−41.0	0.0520	49.0	4.0	4.0
4	45.0	−0.0349	1.0	0.0318	−89.0	46.0	1.0
5	22.5	−0.0354	−22.0	0.0323	68.0	23.0	0.5
6	0.0	−0.0381	−43.0	0.0348	47.0	2.00	2.0

TABLE 5 | Deflection angles of Stacking No. 2 with unit ply angle misalignment in each layer at one time.

Ply No.	Ply angle/°	θ_G/°	θ_{tw}/°	θ_d/°	Ply No.	Ply angle/°	θ_G/°	θ_{tw}/°	θ_d/°
1	0	0	1.0	1.0	7	−30	−30	−28.0	2.0
2	30	30	29.0	−1.0	8	30	30	−61.0	−1.0
3	60	−30	62.0	2.0	9	0	0	−89.0	1.0
4	90	0	−89.0	1.0	10	−30	−30	62.0	2.0
5	−60	30	−61.0	−1.0	11	30	29.0	29.0	−1.0
6	−30	−30	−28.0	2.0	12	0	1.0	1.0	1.0

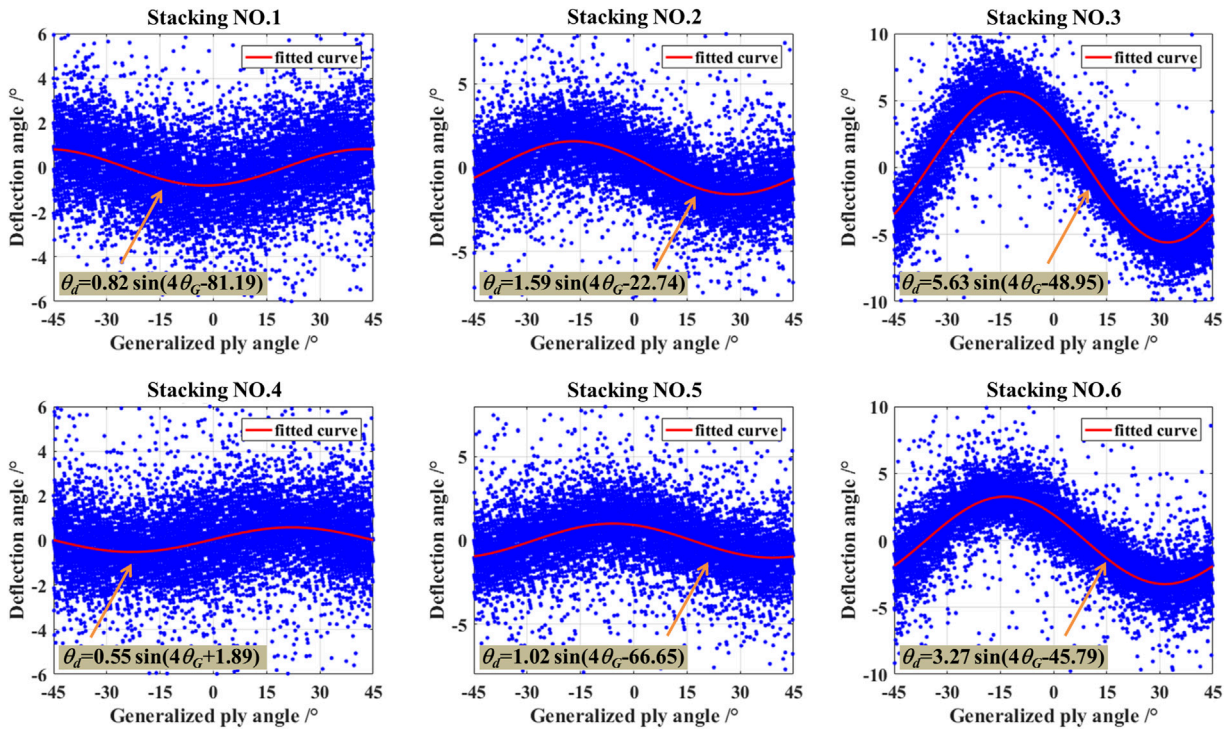

FIGURE 6 | Point diagrams and fitting curves (including fitting functions) of the deflection angle versus the generalized ply angle for Stacking Nos. 1–6.

uniformity of bending stiffness. The smaller the amplitude of the deflection angle, the better is the uniformity of bending stiffness.

4.2 Random Ply Angle Misalignments

Based on stacking sequences in **Table 2**, a series of random numbers were imposed on them. The random numbers were generated from MATLAB and obeyed the normal distribution. The probability density function was defined as follows:

$$f(x) = \frac{1}{\sigma\sqrt{2\pi}} \exp\left(-\frac{(x-\mu)^2}{2\sigma^2} \right), -\infty < x < +\infty, \qquad (13)$$

where μ was the mean value, and σ was the standard misalignment. In this study, the mean value was 0, and σ was set to 1.5.

The combined stacking sequences were sent to Abaqus by applications of Python script and were acted on the space mirror in turn, namely, the Monte Carlo method (Liu et al., 2019). The number of cycles was 10,000. After calculation, responses were extracted, including coordinates and displacements of nodes; then, the data were analyzed by the aforementioned statement.

Diagrams of the deflection angle versus the generalized ply angle are shown in **Figure 6**. The deflection angle changes with the generalized ply angle approximately as a trigonometric function within each laminate.

The fitting curve and function of the deflection angle have been drawn in the diagram. The amplitudes of the fitting functions are different from each other. Amplitudes for Stacking Nos. 1–6 are 0.82, 1.59, 5.63, 0.55, 1.02, and 3.27, respectively. It indicates that Stacking Nos. 1 and 4 are the smallest, Stacking Nos. 3 and 6 are the biggest, and Stacking Nos. 2 and 5 are in the middle.

Therefore, Stacking Nos. 1 and 4 have faster tendencies to the uniform bending stiffness than others. The diagram of deflection angles, especially amplitudes, could be used to compare the consistency of bending stiffness.

Compared to the method of the regularization stiffness coefficient and coefficients of bending/twisting, the deflection angle is a comprehensive value to indicate the relationship between the twisting stiffness and the bending stiffness. It provides an objective way to compare the uniformity of bending stiffness to obtain a laminate with the more uniform bending stiffness.

5 CONCLUSION

By applications of theoretical derivation, simulation, and comparison, it could be concluded that:

1) the principal moment direction is 45° to the generalized ply angle, resulting from the ply angle misalignments;
2) the deflection angle, derived from the angle misalignment, essentially has nothing to do with the angle misalignment and is an inherent property of the laminate;
3) the deflection angle varies from the stacking sequence and is dependent on the generalized ply angle. In addition, it is approximately made of a trigonometric curve and the amplitude of the fitting trigonometric function is a parameter to be compared;
4) the smaller the deflection angle, the better is the uniformity of bending stiffness. Thus, it is an efficient approach to achieve a stacking sequence with more uniformity of bending stiffness by comparing the deflection angle.

Therefore, for a symmetric and quasi-isotropic laminate, we could predict the principal moment and curvature directions resulting from ply angle misalignments and obtain their difference and the deflection angle. It is beneficial to optimize stacking sequences and precisely control the accuracy of the mirror by stacking sequences.

DATA AVAILABILITY STATEMENT

The original contributions presented in the study are included in the article/Supplementary Material, further inquiries can be directed to the corresponding authors.

AUTHOR CONTRIBUTIONS

LL and FS suggested this study, analyzed data, and wrote the manuscript. QL performed the research, analyzed data, and wrote the manuscript. All authors discussed the results and commented on the manuscript.

FUNDING

This work was supported by the National Natural Science Foundation of China (Grant Nos. 11972041 and 11902327) and the Youth Innovation Promotion Association CAS.

REFERENCES

Arao, Y., Koyanagi, J., Utsunomiya, S., and Kawada, H. (2011). Effect of Ply Angle Misalignment on Out-Of-Plane Deformation of Symmetrical Cross-Ply CFRP Laminates: Accuracy of the Ply Angle Alignment. *Compos. Structures* 93 (4), 1225–1230. doi:10.1016/j.compstruct.2010.10.019

Bowers, C. W., Bowers, C. W., Content, D. A., Marzouk, M., and Romeo, R. C. (2000). Advances in Very Lightweight Composite Mirror Technology. *Opt. Eng.* 39 (9), 2320–2329. doi:10.1117/1.1288125

Bruyneel, M., Beghin, C., Craveur, G., Grihon, S., and Sosonkina, M. (2012). Stacking Sequence Optimization for Constant Stiffness Laminates Based on a Continuous Optimization Approach. *Struct. Multidisc Optim* 46 (6), 783–794. doi:10.1007/s00158-012-0806-4

Chen, Y., Ye, L., and Fu, K. (2021). Progressive Failure of CFRP Tubes Reinforced with Composite sandwich Panels: Numerical Analysis and Energy Absorption. *Compos. Structures* 263, 113674. doi:10.1016/j.compstruct.2021.113674

Cheng, L., Gong, P., Wang, Q., Zou, M., Zhang, Y., and Liu, Z. (2021). Effects of Ply Thickness Deviation and Ply Angle Misalignment on the Surface Accuracy of CFRP Laminates. *Compos. Structures* 270, 114073. doi:10.1016/j.compstruct.2021.114073

Fukunaga, H. (1990). On Isotropic Laminate Configurations. *J. Compos. Mater.* 24 (5), 519–535. doi:10.1177/002199839002400504

Fukunaga, H., and Sekine, H. (1992). Stiffness Design Method of Symmetric Laminates Using Lamination Parameters. *AIAA J.* 30 (11), 2791–2793. doi:10.2514/3.11304

Gere, J. M., and Goodno, B. J. (2012). *Mechanics of Materials*. 8th edition edn. Stamford: Cengage Learning.

Hyer, M. W. (1981). Some Observations on the Cured Shape of Thin Unsymmetric Laminates. *J. Compos. Mater.* 15, 175–194. doi:10.1177/002199838101500207

Kim, K.-P., and Hale, R. D. (2010). Composite Mirror Surface Deformation Due to Lay-Up Sequences within Quasi-Isotropic Laminates. *Opt. Eng.* 49 (6), 063002–063010. doi:10.1117/1.3456694

Liu, Q., Cai, Y., Liu, X., Yang, Z., Jiang, S., and Leng, S. (2019). Influence of the Ply Angle Deviation on the Out-Of-Plane Deformation of the Composite Space Mirror. *Appl. Compos. Mater.* 26 (3), 897–911. doi:10.1007/s10443-018-9756-3

Ma, G., Kang, R., Dong, Z., Yin, S., Bao, Y., and Guo, D. (2020). Hole Quality in Longitudinal-Torsional Coupled Ultrasonic Vibration Assisted Drilling of Carbon Fiber Reinforced Plastics. *Front. Mech. Eng.* 15 (4), 538–546. doi:10.1007/s11465-020-0598-y

Różyło, P., and Dębski, H. (2022). The Influence of Composite Lay-Up on the Stability of a Structure with Closed Section. *Adv. Sci. Technol. Res. J.* 16 (1), 260–265. doi:10.12913/22998624/145156

Song, C., and Jin, X. (2021). Fracture Angle Prediction for Matrix Failure of Carbon-Fiber-Reinforced Polymer Using Energy Method. *Composites Sci. Tech.* 211, 108869. doi:10.1016/j.compscitech.2021.108869

Steeves, J., and Pellegrino, S. (2017). Post-cure Shape Errors of Ultra-thin Symmetric CFRP Laminates: Effect of Ply-Level Imperfections. *Compos. Structures* 164, 237–247. doi:10.1016/j.compstruct.2016.12.075

Tanaka, S., Ikeda, T., and Senba, A. (2016). Sensitivity Analysis of thermal Deformation of CFRP Laminate Reflector Due to Fiber Orientation Error. *J. Mech. Sci. Technol.* 30 (10), 4423–4426. doi:10.1007/s12206-016-0905-z

Thompson, S. J., Bichon, S., and Grant, R. J. (2014). Influence of Ply Misalignment on Form Error in the Manufacturing of CFRP Mirrors. *Opt. Mater. Express* 4 (1), 79–91. doi:10.1364/ome.4.000079

Ugural, A. C. (2009). *Stresses in Beams, Plates, and Shells*. Boca Raton: CRC Press.

Vannucci, P., and Verchery, G. (2002). A New Method for Generating Fully Isotropic Laminates. *Compos. Structures* 58 (1), 75–82. doi:10.1016/S0263-8223(02)00038-7

Verchery, G. (2011). Design Rules for the Laminate Stiffness. *Mech. Compos. Mater.* 47 (1), 47–58. doi:10.1007/s11029-011-9186-x

Wei, L., Zhang, L., and Gong, X. (2017). Design and Optimization of the CFRP Mirror Components. *Photonic. Sens.* 7 (3), 270–277. doi:10.1007/s13320-017-0388-2

Wilhelmsson, D., Rikemanson, D., Bru, T., and Asp, L. E. (2020). Compressive Strength Assessment of a CFRP Aero-Engine Component - an Approach Based on Measured Fibre Misalignment Angles. *Compos. Structures* 233, 111632. doi:10.1016/j.compstruct.2019.111632

Wu, K. M., and Avery, B. L. (1992). Fully Isotropic Laminates and Quasi-Homogeneous Anisotropic Laminates*. *J. Compos. Mater.* 26 (14), 2107–2117. doi:10.1177/002199839202601406

Xie, F., Lu, Z., Yang, Z., Hu, W., and Yuan, Z. (2016). Mechanical Behaviors and Molecular Deformation Mechanisms of Polymers under High Speed Shock Compression: a Molecular Dynamics Simulation Study. *Polymer* 98, 294–304. doi:10.1016/j.polymer.2016.06.047

Yang, Z., Tang, Z., Xie, Y., Shi, H., Zhang, B., and Guo, H. (2018). Effect of Lamina Thickness of Prepreg on the Surface Accuracy of Carbon Fiber Composite Space Mirrors. *Appl. Compos. Mater.* 25 (1), 105–112. doi:10.1007/s10443-017-9604-x

Yang, Z., Liu, Q., Zhang, B., Xu, L., Tang, Z., and Xie, Y. (2019). Influence of Layup Sequence on the Surface Accuracy of Carbon Fiber Composite Space Mirrors. *Appl. Compos. Mater.* 26 (1), 219–238. doi:10.1007/s10443-018-9690-4

Yi, X., Du, S., and Zhang, L. (2018). *Fundamentals of Composite Materials*, Vol. 1. Beijing: Chemical Industry Press. doi:10.1007/978-981-10-5696-3

Yoon, J.-S., Kim, H.-I., Han, J.-H., and Yang, H.-S. (2014). Effect of Dimensional Stability of Composites on Optical Performances of Space Telescopes. *J. Aerosp. Eng.* 27 (1), 40–47. doi:10.1061/(asce)as.1943-5525.0000237

Conflict of Interest: The authors declare that the research was conducted in the absence of any commercial or financial relationships that could be construed as a potential conflict of interest.

Publisher's Note: All claims expressed in this article are solely those of the authors and do not necessarily represent those of their affiliated organizations, or those of the publisher, the editors, and the reviewers. Any product that may be evaluated in this article, or claim that may be made by its manufacturer, is not guaranteed or endorsed by the publisher.